Electronic Supplementary Material (ESI) for Nanoscale.

Nonlinear detour phase holography

Bingxia Wang[1], Xuanmiao Hong[1], Kai Wang[1,], Xin Chen[2], Shan Liu[3], Wieslaw Krolikowski[3,4], Peixiang Lu[1,5,6,*] and Yan Sheng[3,*]*

[1]Wuhan National Laboratory for Optoelectronics and School of Physics, Huazhong University of Science and Technology, Wuhan 430074, China

[2]School of Physics and Optoelectronics Engineering, Xidian University, Xi'an 710071, China

[3]Laser Physics Center, Research School of Physics, Australian National University, Canberra, ACT 2601, Australia

[4]Science Program, Texas A&M University at Qatar, Doha 23874, Qatar

[5]Guangdong Intelligent Robotics Institute, Dongguan 523808, China

[6]CAS Center for Excellence in Ultra-intense Laser Science, Shanghai 201800, China

*Corresponding authors: kale_wong@hust.edu.cn (KW), lupeixiang@hust.edu.cn (PXL), yan.sheng@anu.edu.au (YS)

1. Detailed derivation of the nonlinear detour phase method

We consider a general $\chi^{(2)}$ hologram composed of series of basic units. The basic units have the same number of antiparallel ferroelectric domains, but the arrangement of these domains is different for each unit. The coordinates of the (n, m)-th basic unit can be written as ($n\delta_v$, $m\delta_v$), where δ_v is the width and height of the basic unit. We consider the width and height of the inverted domains as $c\delta_v$ and $W_{nm}\delta_v$, and the surrounding area is filled with the $-\chi^{(2)}$ domains. The inverted domain is displaced from the center of the basic unit ($n\delta_v$, $m\delta_v$) by $P_{nm}\delta_v$. We illuminate the $\chi^{(2)}$ hologram with a normal incident monochromatic plane wave with homogeneous amplitude. For the SHG process, the SHG emitted from the positive and negative $\chi^{(2)}$ areas has the same amplitude but a phase difference of π, which imposes a binary phase modulation onto the generated second harmonic light. Therefore, the emitted total second harmonic electric field, $h(v_x, v_y)$, considered as the superposition of the second harmonic electric fields, $h_{nm}(v_{xnm}, v_{ynm})$, emitted from each basic unit, can be written as:

$$h\left(v_x, v_y\right)=\sum_{n,m} h_{nm}\left(v_{xnm}, v_{ynm}\right)=\sum_{n,m} h_0 \cdot \exp\left(\pi i \cdot rect\left(\frac{v_{xnm}-P_{nm}\delta_v}{c\cdot\delta_v}\right) rect\left(\frac{v_{ynm}}{W_{nm}\cdot\delta_v}\right)\right) \tag{S1}$$

where, $v_{xnm}= v_x - n\delta_v$; $v_{ynm}= v_y - m\delta_v$; (v_{xnm}, v_{ynm}) is the coordinate in the basic unit coordinate system; h_0 is the constant amplitude; the products of the *rect* functions accounts for the role of the inverted domains. The Fourier transform of $h(v_x, v_y)$, which represents the complex electric field in the image plane, can be written as the superposition of Fourier transform of $h_{nm}(v_{xnm}, v_{ynm})$:

$$u\left(\mathrm{x}, y\right)=\sum_{n,m} u_{nm}\left(x_{nm}, y_{nm}\right)=\sum_{n,m}\int_{-\infty}^{+\infty}\int_{-\infty}^{+\infty} h_{nm}\left(v_{xnm}, v_{ynm}\right)\exp\left(i2\pi\left(v_{xnm}x_{nm}+v_{ynm}y_{nm}\right)\right)\mathrm{d}v_{xnm}dv_{ynm} \tag{S2}$$

where, (x_{nm}, y_{nm}) is the Fourier space coordinate corresponding to the basic unit coordinate system (v_{xnm}, v_{ynm}). From the sampling theorem we get the largest permissible x_{nm} as:

$$x_{nm}=\frac{1}{\delta_v} \tag{S3}$$

Substitution of Equation (S1) into Equation (S2) gives:

$$u(\mathrm{x},y)=\sum_{n,m}\int_{-\infty}^{+\infty}\int_{-\infty}^{+\infty}h_0\cdot\exp\left(\pi i\cdot\left(rect\left(\frac{v_{xnm}-P_{nm}\delta_v}{c\cdot\delta_v}\right)rect\left(\frac{v_{ynm}}{W_{nm}\cdot\delta_v}\right)\right)\right)$$
$$\cdot\exp\left(i2\pi v_{xnm}x_{nm}\right)\exp\left(i2\pi v_{ynm}y_{nm}\right)dv_{xnm}dv_{ynm} \tag{S4}$$

when $-\frac{c\delta_v}{2}+P_{nm}\delta_v\le v_{xnm}\le\frac{c\delta_v}{2}+P_{nm}\delta_v$, the function $rect\left(\frac{v_{xnm}-P_{nm}\delta_v}{c\cdot\delta_v}\right)$ is equal to 1; otherwise it equals 0.

When $-\frac{W_{nm}\delta_v}{2}\le v_{ynm}\le\frac{W_{nm}\delta_v}{2}$, the function $rect\left(\frac{v_{ynm}}{W_{nm}\cdot\delta_v}\right)$ is equal to 1; otherwise it equals 0. And the follwing constraints should also be mentioned here: $\left|P_{nm}\delta_v\right|+\frac{c\delta_v}{2}\le\frac{\delta_v}{2}$, $W_{nm}\le 1$. Therefore, Equation (S4) can be rewritten as:

$$u(\mathrm{x},y)=h_0\cdot\sum_{n,m}\int_{-\frac{c\delta_v}{2}+P_{nm}\delta_v}^{+\frac{c\delta_v}{2}+P_{nm}\delta_v}\int_{-\frac{W_{nm}\delta_v}{2}}^{+\frac{W_{nm}\delta_v}{2}}\exp(\pi i)\exp\left(i2\pi v_{xnm}x_{nm}\right)\exp\left(i2\pi v_{ynm}y_{nm}\right)dv_{xnm}dv_{ynm} \tag{S5}$$

$$\begin{aligned}u(\mathrm{x},y)&=h_0\exp(\pi i)\sum_{n,m}\int_{-\frac{c\delta_v}{2}+P_{nm}\delta_v}^{+\frac{c\delta_v}{2}+P_{nm}\delta_v}\int_{-\frac{W_{nm}\delta_v}{2}}^{+\frac{W_{nm}\delta_v}{2}}\\&\exp\left(i2\pi v_{xnm}x_{nm}\right)\exp\left(i2\pi v_{ynm}y_{nm}\right)dv_{xnm}dv_{ynm}\\&=h_0\exp(\pi i)\left(\frac{1}{i2\pi}\right)^2\sum_{n,m}\int_{-\frac{c\delta_v}{2}+P_{nm}\delta_v}^{+\frac{c\delta_v}{2}+P_{nm}\delta_v}\int_{-\frac{W_{nm}\delta_v}{2}}^{+\frac{W_{nm}\delta_v}{2}}\exp\left(i2\pi v_{xnm}x_{nm}\right)\\&\exp\left(i2\pi v_{ynm}y_{nm}\right)d\left(i2\pi v_{xnm}\right)d\left(i2\pi v_{ynm}\right)\\&=h_0\exp(\pi i)\left(\frac{1}{i2\pi}\right)^2\\&\sum_{n,m}\left[\exp\left(i2\pi v_{xnm}x_{nm}\right)\Big|_{-\frac{c\delta_v}{2}+P_{nm}\delta_v}^{+\frac{c\delta_v}{2}+P_{nm}\delta_v}\exp\left(i2\pi v_{ynm}y_{nm}\right)\Big|_{-\frac{W_{nm}\delta_v}{2}}^{+\frac{W_{nm}\delta_v}{2}}\right]\end{aligned} \tag{S6}$$

$$u(\mathrm{x},y)=h_0\exp(\pi i)\left(\frac{1}{i2\pi}\right)^2$$
$$\cdot\sum_{n,m}\left[\begin{array}{l}\left(\exp\left(i2\pi\left(+\frac{c\delta_\nu}{2}+P_{nm}\delta_\nu\right)x_{nm}\right)-\exp\left(i2\pi\left(-\frac{c\delta_\nu}{2}+P_{nm}\delta_\nu\right)x_{nm}\right)\right)\\ \cdot\left(\exp\left(i2\pi\frac{W_{nm}\delta_\nu}{2}y_{nm}\right)-\exp\left(-i2\pi\frac{W_{nm}\delta_\nu}{2}y_{nm}\right)\right)\end{array}\right]$$

$$=h_0\exp(\pi i)\left(\frac{1}{i2\pi}\right)^2$$
$$\cdot\sum_{n,m}\left[\exp(i2\pi x_{nm}P_{nm}\delta_\nu)\cdot 2i\sin\left(2\pi\frac{c\delta_\nu}{2}x_{nm}\right)\cdot 2i\sin\left(2\pi y_{nm}\frac{W_{nm}\delta_\nu}{2}\right)\right]$$
$$=h_0\exp(\pi i)\left(\frac{1}{i2\pi}\right)^2(2i)^2$$
$$\cdot\sum_{n,m}\left[\sin\left(2\pi\frac{c\delta_\nu}{2}x_{nm}\right)\sin\left(2\pi y_{nm}\frac{W_{nm}\delta_\nu}{2}\right)\cdot\exp(i2\pi x_{nm}P_{nm}\delta_\nu)\right]$$
$$=\mathrm{const}\cdot\sum_{n,m}\left[\sin\left(2\pi\frac{c\delta_\nu}{2}x_{nm}\right)\sin\left(2\pi y_{nm}\frac{W_{nm}\cdot\delta_\nu}{2}\right)\cdot\exp(i2\pi x_{nm}P_{nm}\delta_\nu)\right]$$

(S7)

Equation (S7) can be rewritten as:

$$u(\mathrm{x},y)=\sum_{n,m}\left[A_{nm}\exp(i2\pi x_{nm}\delta_\nu P_{nm})\right] \quad \text{(S8)}$$

where, $A_{nm}=\mathrm{const}\cdot\sin\left(2\pi\frac{c\delta_\nu}{2}x_{nm}\right)\sin\left(2\pi y_{nm}\frac{W_{nm}\delta_\nu}{2}\right)$ represents the amplitude of emitted SHG from the (*n*, *m*)-th basic unit. In order to simplify the process without sacrificing the conversion efficiency, we choose W_{nm}=1 and c=1/2. Substitution of Equation (S3) into Equation (S8) gives:

$$u(\mathrm{x},y)=\sum_{n,m}\left[A_{nm}\exp(i2\pi P_{nm})\right] \quad \text{(S9)}$$

The desired SHG field at far field can also be expressed as its general form:

$$u'(\mathrm{x},y)=\sum_{nm}A'_{nm}\exp(i\varphi_{nm})\propto\sum_{nm}\exp(i\varphi_{nm}) \quad \text{(S10)}$$

The equalization of the phase term in Equation (S9) and phase in Equation (S10) leads to a simple equation:

$$P_{nm} = \frac{\varphi_{nm}}{2\pi} \tag{S11}$$

where, φ_{nm} is the phase shift of transmitted SHG at far field given by the (n, m)-th basic unit. It shows the SHG phase shift (φ_{nm}) from the (n, m)-th unit is determined by the distance between the center of the inverted domain and the center of the basic unit (P_{nm}) .

2. Measurement of mean diameter of randomly distributed ferroelectric domains

For a particular distributed random domain pattern with average domain diameter, D_{max} , the Fourier transform of the domain pattern gives the G spectrum with a corresponding mean value G_{max}. The quantitative relationship between these two parameters can be connected with formula $D_{max} = \pi / G_{max}$ [S1]. The phase image obtained by the Atomic Force Microscope (Bruker Dimension Edge) in the Piezoelectric Force Microscope (PFM) mode is shown in Figure S1a, where the light yellow represents the "up" domain and dark brown represents the "down" domain. The 2D reciprocal lattice vector G spectrum of the antiparallel domain structure, obtained as Fourier transform of the spatial ferroelectric domain pattern, is plotted in Figure S1b. The corresponding distribution of the magnitude of the reciprocal vector G is demonstrated in Figure S1c, where the average G value is G_{max}=30 μm^{-1}. The resulting average domain diameter corresponding to G_{max} is $D_{max} = \pi / G_{max}$ = 100 nm [S1].

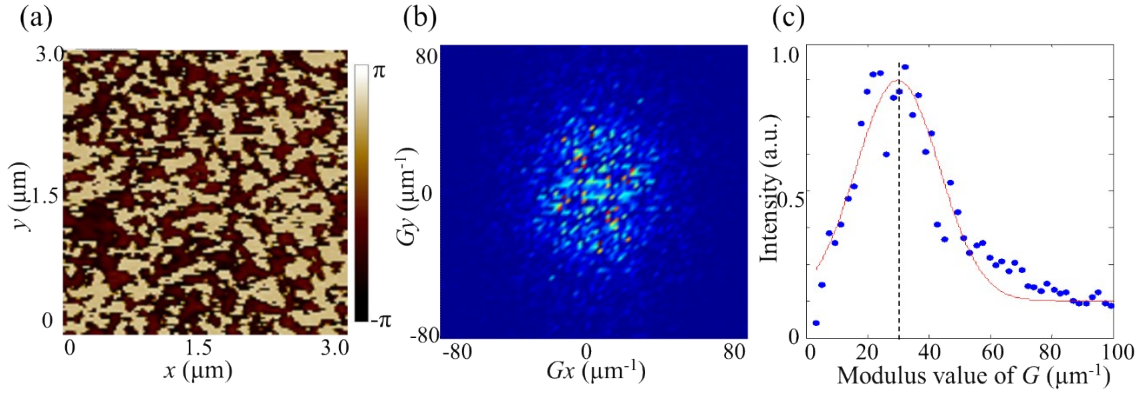

Figure S1. The measurement of mean diameter of randomly distributed ferroelectric domains in as-grown SBN-75 crystal. (a) The phase image obtained by the Atomic Force Microscope (Bruker Dimension Edge) in the Piezoelectric Force Microscope (PFM) mode. (b) 2D reciprocal lattice vector G spectrum of the antiparallel domain structure, obtained as Fourier transform of the spatial ferroelectric domain pattern. (c) The corresponding distribution of the magnitude of the reciprocal vector G. The maximum corresponds to the reciprocal vector with G_{max}=30 μm^{-1}. The resulting average domain diameter corresponding to G_{max} is $D_{max} = \pi / G_{max}$ = 100 nm.

3. High-quality nonlinear holographic imaging of letter ‘H’

We have performed numerical simulations to obtain quality-improved holographic imaging of letter ‘H’ with the nonlinear detour phase method by increasing the pixel number of phase plate and the fabrication accuracy, as shown in Figure S2. The left and right columns show the holographic image from the same-sized holograms (304 μm × 304 μm) but with different pixel numbers and fabrication resolutions, respectively. Figure S2a shows the SHG phase map with 4548 pixels in total. The reconstructed hologram is shown in Figure S2b with 1 μm resolution. The bottom inset is the enlarged hologram pattern within the marked pink frame, where the stripe-shaped inverted domain patterns reflecting the characteristics of nonlinear detour phase method can be clearly seen. In this case, the width of each basic unit (P_1, P_2, P_3, P_4) is 4 μm. Figure S2c presents the simulated nonlinear holographic image. It can be clearly seen that with the increased number of pixels the image quality of the nonlinear detour hologram (4548 pixels) becomes better than that presented in Figure 3c (1124 pixels). To further improve the holographic image, we increase the fabrication resolution 2 times and keep the hologram size unchanged. Then the width of each basic unit (P_1, P_2, P_3, P_4) is 2 μm and the phase plate contains a total of 18168 pixels. The corresponding phase map at the hologram plane is shown in Figure S2d, and the SHG hologram composed of narrower inverted domains is presented in Figure S2e. Figure S2f shows the simulated nonlinear holographic image. It can be clearly seen that with the increased fabrication accuracy the holographic image is further improved.

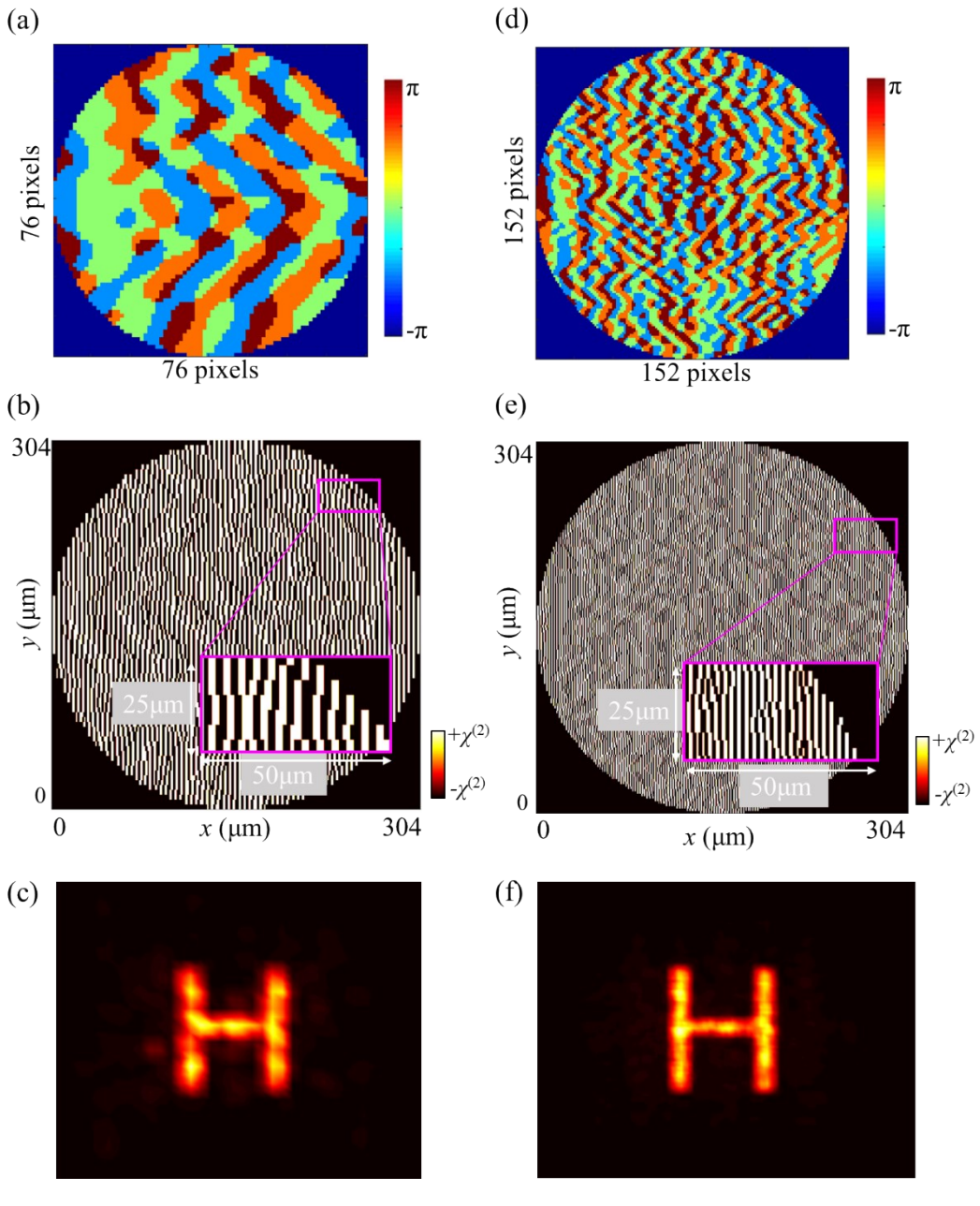

Figure S2. Numerical simulations of quality-improved holographic imaging of letter 'H' with the proposed nonlinear detour phase method by increasing the pixel number of phase plate and fabrication accuracy. (a, b, c) When the fabrication resolution is 1 μm, the calculated SHG phase map (a), the reconstructed hologram (b) and the simulated nonlinear holographic image (c). (d, e, f) When the fabrication resolution is 0.5 μm, the numerically calculated SHG phase map (d), the reconstructed hologram (e) and the simulated nonlinear holographic image (f).

4. Comparison of holographic images reconstructed by nonlinear detour phase hologram and nonlinear binary phase hologram

We have performed the numerical simulations of holographic image of '*hot coffee*' reconstructed by the nonlinear binary phase hologram[S2] and the proposed nonlinear detour phase hologram (considering the same pixel number of phase plate and 1-μm fabrication resolution) as presented in Figure S3. Specifically, Figure S3a presents the simulation result

with nonlinear binary phase hologram. The top row shows the amplitude and phase of the Fourier transform of the desired wavefront (the target '*hot coffee*' image is shown in the insert). The reconstructed binary phase hologram and the enlarged pattern at the marked area is shown in the middle row. The simulated nonlinear holographic image is displayed in the bottom row. For comparison, Figure S3b presents the simulation result with nonlinear detour phase hologram. It can be clearly seen, the imaging quality of nonlinear detour phase hologram is superior to the general nonlinear binary phase hologram.

The nonlinear binary phase hologram is a general method for reconstructing holographic imaging. The calculated nonlinearity modulation pattern is always as complicated as 'Quick Response (QR) codes' due to the direct Fourier transform of the desired wavefront. Therefore, using the actual fabrication accuracy (which is 1 μm in this case) to approach this complicated pattern will induce large processing errors, which usually results in low quality holographic imaging. To solve this problem, one can optimize the nonlinear hologram to make it compatible with the experimentally achieved fabrication resolution. The proposed nonlinear detour phase hologram is a simple and effective method due to its highly simplified pattern, which can be reconstructed with experimentally achieved fabrication accuracy. To sum up, nonlinear binary phase hologram is always accompanied by large processing errors leading to a low holographic imaging quality, while as a simple and effect method this proposed nonlinear detour phase hologram plays an important role in improvement of image quality.

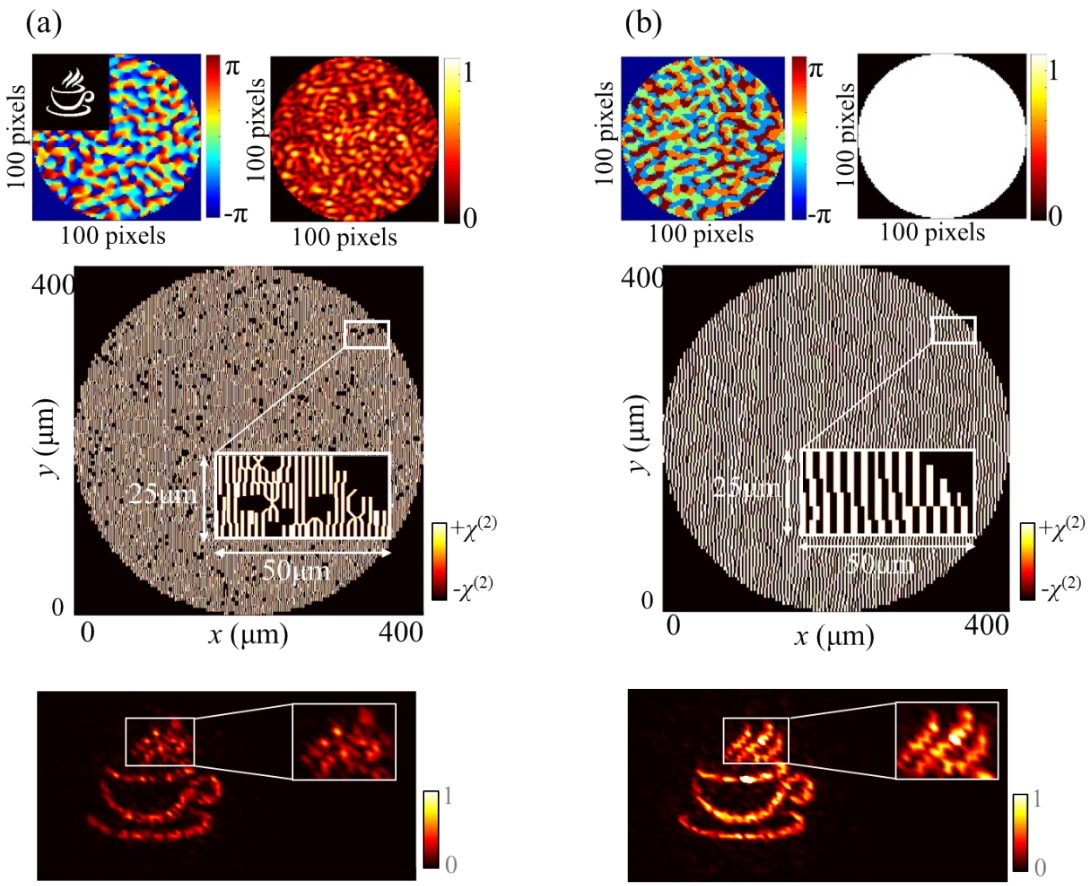

Figure S3. Comparison of the holographic images of '*hot coffee*' reconstructed by nonlinear binary phase hologram and nonlinear detour phase hologram (pixel number of phase plate and fabrication resolution setting as 7860 and 1-μm). (a) Simulation result with nonlinear binary phase hologram. (b) Simulation result with nonlinear detour phase hologram. (Up row) The calculated phases and amplitudes at hologram plane. (Middle row) The reconstructed holograms and the expanded view of hologram pattern at the marked areas. (Bottom row) The simulated nonlinear holographic images and expanded view of the marked area. Clearly, holographic image quality of nonlinear detour phase hologram is superior to nonlinear binary phase hologram.

References

[S1] B. Wang, K. Switowski, C. Cojocaru, V. Roppo, Y. Sheng, M. Scalora, J. Kisielewski, D. Pawlak, R. Vilaseca, H. Akhouayri, W. Krolikowski, and J. Trull, *Opt. Express*, 2018, **26**, 1083-1096.

[S2] A. Shapira, R. Shiloh, I. Juwiler and A. Arie, Opt. Lett., 2012, 37, 2136-2138